

Dynamic characteristics of saturated loess under different confining pressures: a microscopic analysis

Huie Chen¹ · Yaling Jiang¹ · Cencen Niu¹  · Guanjun Leng¹ · Guili Tian¹

Received: 1 March 2017 / Accepted: 10 June 2017 / Published online: 24 July 2017
© Springer-Verlag GmbH Germany 2017

Abstract To explore the influence of confining pressure on the dynamic characteristics of saturated loess and variation of the characteristics in micro-mechanisms therein, dynamic triaxial testing of loess from Xianyang was carried out. The dynamic elastic modulus of saturated loess after different numbers of cycles was available through the test and the relationship between the dynamic elastic modulus and confining pressure can be analysed. A scanning electron microscope (SEM) examination was conducted to assess the microstructural characteristics of the specimens. From both qualitative and quantitative aspects, the variations in microstructure were analysed. The microstructural parameters which had greater correlation with macroscopic strength were found based on grey relationship theory, then the relationship between them was found by curve-fitting. The results show that, the dynamic elastic modulus of saturated loess was increased as the confining pressure increases, but decreased with increasing vibration cycle and tended to be stable over time. The approximate microstructural parameters selected were correlated to the dynamic elastic modulus in addition to the average pore shape factor; because of the high correlation with the dynamic elastic modulus, the average diameter of the pores, the average shape factor and fractal dimension of the morphology of structural units were selected to fit the dynamic elastic modulus.

Keywords Saturated loess · Dynamic elastic modulus · Microstructure · Quantitative analysis · Grey correlation degree

✉ Cencen Niu
niucencen@jlu.edu.cn

¹ College of Construction Engineering, Jilin University, Changchun 130026, China

Introduction

As a kind of special soil, loess was formed in the Quaternary, and is widespread in areas such as the American Midwest, Southern Russia, Northern France, Central and Western Europe and so on. China has one of the most widespread deposits of loess in the world, accounting for about 6.8% of the land area, and it is mainly distributed in the Northwest of China (Liu 1965) which is always of high-seismic intensity and is an earthquake-prone area. In this area, several M8 earthquakes have occurred, small and medium-magnitude earthquakes also occur frequently (Shi 2003). With the implementation of a western development strategy in China, the amount of engineering construction in the loess area will gradually increase, obviously the stability of loess is very important in construction. Accordingly, it is worth studying its dynamic characteristics. The engineering properties of soil are mainly controlled by the microstructure thereof (Terzaghi and Peck 1948; Osipov 1985), and the dynamic characteristics of soil, especially the strength, have a significant correlation with the structural characteristics.

Recent research on the dynamic strength and microstructure of loess has made some progress. The influence of consolidation ratio on dynamic strength and microstructure of loess was studied by Xiao et al. (2009) through use of a dynamic triaxial test. To explore the liquefaction characteristics of loess, Wang et al. (2012b) carried out microstructural investigations and dynamic triaxial tests on the loess from different regions. Wang et al. (2012a, 2013) discussed the dynamic strength characteristics of Lishi and Malan loess through dynamic triaxial test data. Using a resonant column test on loess samples, Mosallamy et al. (2015) explored the effect of void ratio, water content and silt content on the maximum shear modulus and damping ratio. Static and dynamic triaxial tests, seismic subsidence

and collapsibility tests were done by Yan and Huang (2014) to study the effect of water content on static and dynamic strength, collapse settlement and rebound modulus. In the quantitative analysis of the microstructure of loess, Jiang et al. (2014) studied the microstructure of undisturbed and remoulded loess before, and after, conventional triaxial compression testing and reduced triaxial compression testing using mercury intrusion porosimetry (MIP) and scanning electron microscopy (SEM). The particle-size composition and mineralogical composition of loess in central Spain were measured by Giménez (2012), and the relationship between mineralogical composition and microstructure was discussed by qualitative analysis of microstructure. Through unconsolidated-undrained dynamic triaxial tests on a slide-zone loess and a quantitative analysis of the microstructure of a loess after dynamic testing, Wang et al. (2014) found a relationship between dynamic strength and pore microstructure of loess in a slide zone. Hu et al. (2001) studied the influence of dynamic load on the shear strength of loess by dynamic compaction test, and explored the relationship between shear strength and microstructure by quantitative analysis of microstructure. These results are all important for the understanding of the dynamic characteristics and the microstructure of loess, but in terms of dynamic characteristics, most of the existing results focus on the macro-perspective in that they explore the dynamic characteristics at different water contents and loading methods. From the perspective of microstructure, most results are derived under static load regimes. Only rarely has microstructure analysis been done after dynamic testing, or only the pore microstructure was analysed or its dynamic load could not represent seismic random load events. Therefore, it will be useful for understanding the dynamic characteristics of loess to explore its macroscopic strength from the perspective of microstructure under a suitable dynamic load regime, so as to provide some theoretical basis for practical engineering works. Due to the variation of consolidation pressure at different depths, and it inevitably having an effect on the dynamic characteristics, here, the dynamic characteristics of a saturated loess under different confining pressures were studied from the microscopic perspective, and the correlation between microstructural parameters and macroscopic strength was evaluated.

Sample properties and test procedure

Sample properties

The loess was taken from Qinsong village, Xinglong town, Xianyang Count, Shanxi Province (Fig. 1), from a vertical depth of 4 m. The physical parameters and particle-size composition of samples are respectively shown in Tables 1 and 2.

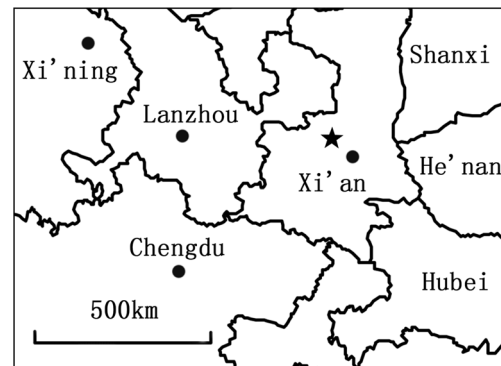


Fig. 1 Sampling location

According to the data in Tables 1 and 2, the silt (0.075 ~ 0.005 mm) content of the sample is 72.55%, the clay (<0.005 mm) accounted for 26.15% by mass, the plasticity index was 15, and it was thus classified as a low liquid limit clay on the basis of ASTM standards (ASTM D2487-11 2011). Additionally, the loess is classified as collapsible (the initial collapse pressure is 178 kPa (Luo et al. 2004)). Since the mineral composition affects the engineering geological properties of a soil, the mineral composition was measured by X-ray diffraction (Table 3). The primary mineral content in the loess is 78%, and the quartz and feldspar contents are high, therefore conferring good resistance to weathering.

Test procedure

A TAJ-20 type soil dynamic triaxial testing machine made by Tianshui Hongshan Testing Machine Co. Ltd. was used for this dynamic test. The undisturbed loess was prepared as standard size samples: ϕ 39.1 mm \times h 80 mm, then the samples were vacuum saturated. The saturated water content is 36.2%, and the degree of saturation of samples is greater than 97%.

While studying seismic load effects, the frequency of dynamic loading is generally 1 to 4 Hz, and we measure and record the axial stress and strain under undrained conditions until the axial strain reaches a pre-specified failure criterion (Li 2004). The dynamic triaxial test in this paper was carried out under undrained conditions, and the dynamic load was sinusoidal at 1 Hz. It is necessary to study the dynamic characteristics of soil under different confining pressures since the consolidation pressure of loess varies with depth. The initial collapse pressure was 178 kPa, to avoid collapse of the specimens, the confining pressures were 80, 100, 120 and 140 kPa, and the amplitude was 30 kPa. For anisotropic consolidation, the failure mode of soil is not of a single type, but is closely related to dynamic load and static conditions (Li 2004). Therefore, a consolidation ratio $K_c = 1$ was chosen to eliminate the influence of different failure modes on the microstructure of the soil; the specific testing programme is shown in Table 4. Dynamic testing was halted when the axial strain

Table 1 Physical parameters of the sample

Soil natural density $\rho(\text{g}/\text{cm}^3)$	Natural water content $\omega(\%)$	Void ratio e	Degree of saturation $S_r(\%)$	Liquid limit $\omega_L(\%)$	Plastic limit $\omega_P(\%)$	Plasticity index I_P	Specific gravity G_s
1.62	20.28	1.01	54	34	19	15	2.71

reached the failure criterion $\varepsilon_d = 5\%$ (Li 1990). The SEM specimens (vertical section) were cut from the damaged dynamic test specimens. Then the microstructure of each specimen under different confining pressures was evaluated.

The classical method of testing and analysis under random load, such as is imposed by seismic events, is to make the random load equal to the harmonic with same amplitude under different vibration cycles, then the experiments and analysis are carried out under that harmonic. For seismic loading, in the input and calculation, the amplitude of the harmonic is equal to 0.65 times the maximum amplitude of the seismic stress. The correspondence between magnitude and the equivalent action cycle is shown in Table 5. As the earthquake fortification intensity of Xianyang is 7 degrees, the magnitude of earthquake happening in this area is no higher than 7 in general, so 12 was chosen as the number of equivalent action cycles according to Table 5, then the first 12 cycles of variation of the data were analysed.

Firstly, we put the saturated loess sample into a sample loading tube surrounded by a latex film, then placed them on the bottom pressure head in the pressure chamber. A rubber band was used to bind the latex film to the pressure head to prevent leakage of water (as shown in Fig. 2), and then the sample loading tube was removed. Then we lowered the pressure chamber to the pedestal and locked it (Fig. 3). We opened the air outlet to proceed the hardware resetting process through the use of the control software (the interface thereof is shown in Fig. 4); the aim of hardware resetting was to eliminate the error caused by the machine. We closed all drain valves, opened the water injection valve to inject water into the pressure chamber, and after the pressure chamber had been filled, closed the air outlet. Then the confining pressure was applied to the sample through the lateral control option in the controlling software (at a rate of 0.1 kPa/s), meanwhile, drain valve 2 was opened to allow consolidation. The volume of water in the volume change tube was recorded every hour. Consolidation was considered to be completed when the volume change was less than 0.01 ml. Then drain valve 2 was closed, and dynamic load was applied by the axial control option in the controlling software. As the failure criterion was met, the dynamic test was deemed to have been completed.

Dynamic characteristics

As shown in Fig. 5, the failure mode of the specimens is a tensile failure, and the failure location is always in the middle

of the specimen. This is due to the fact that, when the axial pressure is equal to the confining pressure, the initial effective normal stress acting on the surface at 45 degrees is $\sigma'_0 = (\sigma_{1c} - \sigma_{3c}) / 2 - u_0$ (u_0 is the initial pore water pressure), and the initial effective shear stress is $\tau'_0 = (\sigma_{1c} - \sigma_{3c}) / 2 = 0$. When the confining pressure is constant, the axial cyclic dynamic load is $\pm\sigma_d$, and the increased dynamic shear stress on the 45-degree surface is $\pm\sigma_d/2$: because the compressive strength is significantly higher than the tensile strength, the failure of specimen is tensile.

The data from the first 12 cycles of each specimen were analysed respectively, and the hysteresis curves were plotted. The slope of the connection between the two vertices of the curve was the dynamic elastic modulus (E_d) of the specimen over one cycle. The $E_d - N$ curve can be obtained from the dynamic elastic modulus corresponding to vibration cycles (N). Figure 6 shows the curve of the dynamic elastic modulus under different confining pressures.

Figure 6 shows that the dynamic elastic modulus of this saturated loess decreases gradually with the increasing vibration cycle, but rapidly decreases in the early stages of vibration. In the first three cycles, the dynamic elastic modulus of specimens under confining pressures of 80 kPa and 100 kPa were respectively decreased to 64.8% and 81.0% of their maximum value. This is because the structural strength is the main part of the soil strength in the early stage of vibration, and the vibration significantly influences the soil structure, so the dynamic elastic modulus was greatly reduced. With increasing vibration cycle, the dynamic elastic modulus decreased slowly and the $E_d - N$ curve tends to be stable. Under low confining pressures, the dynamic elastic modulus was not obviously changed after stabilisation, but did change when the confining pressure was high. This may have been due to the soil compaction changing little when the confining pressure was low, the structure was relatively loose, therefore the dynamic elastic modulus altered little. Conversely, at high confining pressures, the larger units were destroyed, and the soil was densified, so the dynamic elastic modulus increased compared with that at low confining pressures.

Table 2 Particle-size distribution

Sand (mm) 2 ~ 0.075	Silt(mm) 0.075 ~ 0.005	Clay (mm) < 0.005
1.3	72.55	26.15

Table 3 Mineral composition content of undisturbed soil

Relative contents of mineral $\omega(B)/10^{-2}$						
Q	fs	Pl	Cc	Do	I	Ch
47	4	8	18	1	15	7
Comment:Q-Quartz	fs-Alkali feldspar	Pl-Plagioclase	Cc-Calcite	Do-Dolomite	I-Illite	Ch-Chlorite

E_{dmax} is the dynamic elastic modulus over the first period of the sample load regime, which is the maximum of dynamic elastic modulus. Figure 7 shows the change in maximal dynamic elastic modulus with the confining pressure.

Figure 7 shows that the maximum dynamic elastic modulus of saturated loess in Xianyang is strongly affected by confining pressure. With increased confining pressure, the dynamic elastic modulus increases, and the increment gradually increases. When the confining pressure increased from 80 kPa to 100 kPa, the increment of E_{dmax} was 1.4%, but was 149.3% while the confining pressure increased from 120 kPa to 140 kPa.

Qualitative analysis of microstructure

In the process of dynamic loading, the axial strain is much larger than the transverse strain, therefore to observe the changes in the axial structure of the specimens, the SEM specimens (vertical section) were respectively taken from damaged parts of Specimens 1 to 4. Meanwhile the microstructure of the undisturbed loess was tested. An XL30 scanning electron microscope (FEI, USA) was used to image the microstructure of the undisturbed loess and SEM specimens were taken from the damaged dynamic specimens. Figure 8 shows photographs of the vertical section of undisturbed loess and SEM specimens 1 to 4 at $1000\times$ magnification.

It can be seen in Fig. 8 that the undisturbed loess has a skeletal structure, and the skeleton is mainly made of silt. The outline of the particles is clear, and the clay particles between the skeleton have a certain role in connectivity (as marked in red in the photograph of the undisturbed loess in Fig. 8). The contact between particles is mainly point contact, and the pores are mainly trellis pores. Compared with undisturbed loess, the structure of Specimen 1 changes little, and a small amount of clay particles are attached to the silt grains. Specimens 2 to 4 retain their skeleton structure, but the number of trellis pores decreases, the number of intergranular

pores and small pores increases, and the clay particle content increases. The silt grains are in direct contact with each other, more clay particles are attached to the soil skeleton, the outline of the particles gradually becomes blurred, and the contact between particles gradually changes to surface contact.

Quantitative analysis of microstructure

The microstructural parameters of samples were studied, and the influence of confining pressure on the dynamic characteristics of the loess was discussed based on the quantitative analysis of microstructure. The Image-Pro Plus (IPP) software for image processing was used to obtain binarised images from the microstructure photographs, and separate the structural units and pores from the images. The core of binarisation is the selection of an image threshold. In this paper, the grey value of each image was transformed into the value corresponding to the mean value of the normal distribution, which was taken as the threshold value for binarisation.

To reflect the influence of the structural unit and pore characteristics on the macroscopic strength, five microstructural parameters were chosen to describe the size, shape, morphological characteristics, directionality and pore content in the structural units. They are the equivalent diameter, average shape factor, the fractal dimension of the morphology, the directional probability entropy and the rate of internal pore. In this paper, several SEM images of the same specimen were analysed and the mean value was taken as the final result.

Significance of microstructural parameters

Equivalent diameter

The equivalent diameter (D) is the diameter of the circle whose area is equal to the area of the structural unit or pore, so that the size of the unit or pore can be described by Eq. (1) (Yuan 2015):

Table 4 Testing programme

Specimen number	1	2	3	4
Confining pressure/ kPa	80	100	120	140
Amplitude/ kPa	30	30	30	30

Table 5 Magnitude-equivalent action cycles (Zhang and Xie 1989)

Magnitude/M	5.5 to 6	6.5	7.0	7.5	8.0
Equivalent action cycles	5	8	12	20	30



Fig. 2 Process of installation sample

$$D = \sqrt{4S/\pi} \tag{1}$$

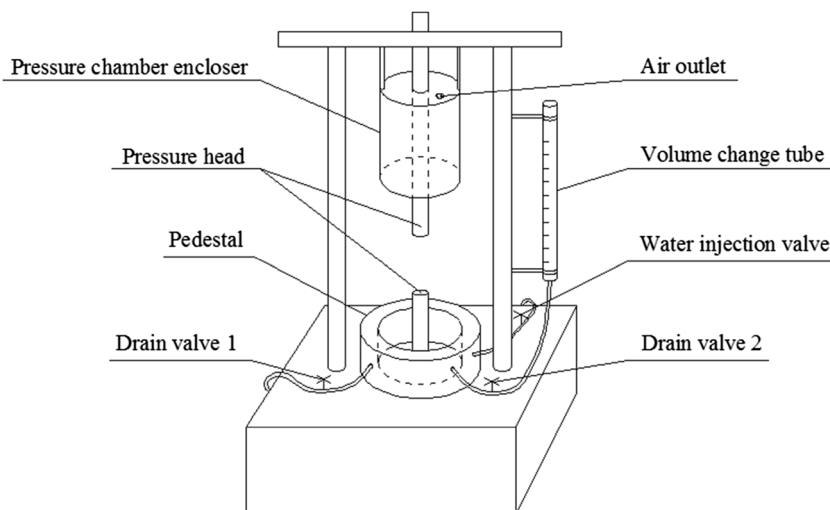
Directional probability entropy

The directional probability entropy (H_m) is a quantitative parameter which can reflect the directionality of structural units and pores, so that the arrangement of units and pores can be described. The directional probability entropy is defined by (Shi 1997):

$$H_m = - \sum_{i=1}^n F_i(\alpha)(\alpha) \log_n F_i(\alpha) \tag{2}$$

Where $F_i(\alpha) = \frac{n_\alpha}{n}$, n_α is the number of the orientation angle which is in the range $[\theta_i \theta_{i+1}]$, and n is the total number of structural units or pores. The value of H_m is in the range

Fig. 3 Schematic diagram of the dynamic triaxial testing machine



$[0,1]$, the greater the value, the worse the directionality of units or pores, conversely the better the directionality.

Average shape factor

To describe the variation in the shape of the structural units or pores, the average shape factor (F) is selected for analysis:

$$F = \frac{1}{n} \sum_{i=1}^n F_i \tag{3}$$

Where $F_i = \frac{P}{S}$, P is the perimeter of the circle whose area is equal to that of structural units or pores, S is the actual perimeter of the units or pores, and n is the total number of units or pores. The value of F is in the range $[0,1]$, the greater the value, the smoother the shape, conversely the longer and narrower it is.

Fractal dimension of morphology

In fact, soil has the characteristic of a statistically self-similar fractal structure, the self-similarity method is used to describe the fractal characteristic of a complex soil, which can reveal the deformation and mechanical behaviour of the soil (Wang and Wang 2000). To analyse the surface characteristics of the structural units and their influence on the macroscopic strength, the fractal dimension of the morphology (B) is obtained by the equivalent area and perimeter method proposed by Moore and Donaldson (1995), then the surface characteristics of units are analysed. The fractal dimension of morphology is calculated as follows:

$$\text{Log}(Perimeter) = \frac{B}{2} \times \text{Log}(Area) + C \tag{4}$$

Where the perimeter and area are the equivalent perimeter and area of the unit or pore, B is the fractal dimension of

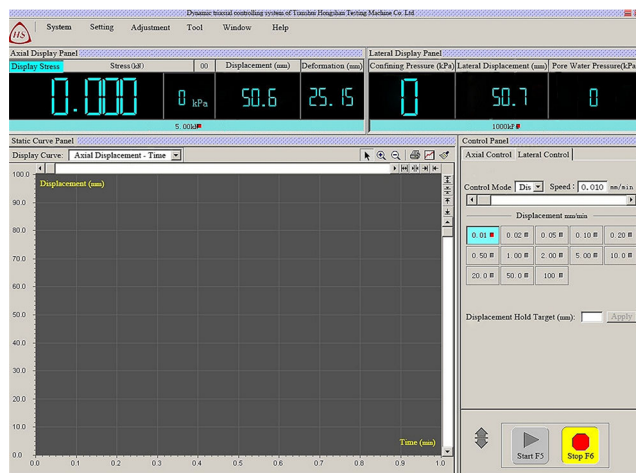


Fig. 4 Control software interface

morphology of unit or pore, and C is the fitting constant. The value of B is between 1 and 2, the greater the value, the more complex the structure of the unit or pore, and accordingly the surface undulations are both rougher and larger.

Rate of internal pore

To describe the pore content in the structural unit, and explore its relationship with macroscopic strength, the rate of internal pore (R) is defined in this paper, and its mean value for each structural unit is taken as the final rate of internal pore. Although R is defined on the basis of a two-dimensional SEM image, to some extent it can represent the internal pore content in units in three-dimensional space since the structural unit is small. R is calculated as follows:

$$R = \frac{S_h}{S} \times 100\% \quad (5)$$

Where S_h is the area of the pores in the structural unit, and S is the total area of the structural unit.

Quantitative analysis of structural units

Equivalent diameter

According to Eq. (1), the equivalent diameter (D) of the structural units can be obtained, and its mean value over all units is taken as the average diameter (\bar{D}) (Table 6).

It can be seen from Table 6 that there are more structural units with equivalent diameters between 5 to 10 μm , and the second most common are larger than 10 μm . With increasing confining pressure, the content of the structural units with an equivalent diameter of less than 2 μm increases, however the number of units in the range 2 to 5 μm remains unchanged. The number of units in the range 5 to 10 μm changes little, but decreases among those greater than 10 μm . The average diameter of the



Fig. 5 Typical tensile failure

units decreases with increasing confining pressure. When the confining pressure increased from 80 kPa to 100 kPa, the average diameter decreased, and the confining pressure continued to increase, the average diameter decreased little. In general, the structural units became smaller. Compared with the undisturbed sample, in specimens 1 to 3, the amount of units with an equivalent diameter of less than 2 μm increased little, and the reduction was mainly among those units with an equivalent diameter greater than 10 μm , and the number of units in the range 5 to 10 μm decreased. This shows that, under low confining pressures, the units which were damaged were mainly those parts with an equivalent diameter greater than 10 μm , and there was little difference in the equivalent diameter distribution between specimens 1 and 2, which may be the reason why the dynamic elastic modulus of specimens 1 and 2 was almost identical. However compared with the undisturbed loess, when $\sigma_3 = 140$ kPa, the structural units with an equivalent diameter of less than 2 μm increased greatly, but the units with equivalent diameters exceeding 10 μm significantly decreased, and the units with equivalent diameters between 5 and 10 μm also decreased. This shows that, during consolidation, the high confining pressure caused significant destruction of the structural units, which increased the number of small particles. Under the action of dynamic load, the pores were compressed, and the small particles in-fill the pores which made the soil specimens more dense, so the dynamic elastic modulus increased.

Directional probability entropy

According to Eq. (2), the directional probability entropy (H_m) of the structural units of each sample can be obtained, as shown in

Fig. 6 E_d -N curve under different confining pressure

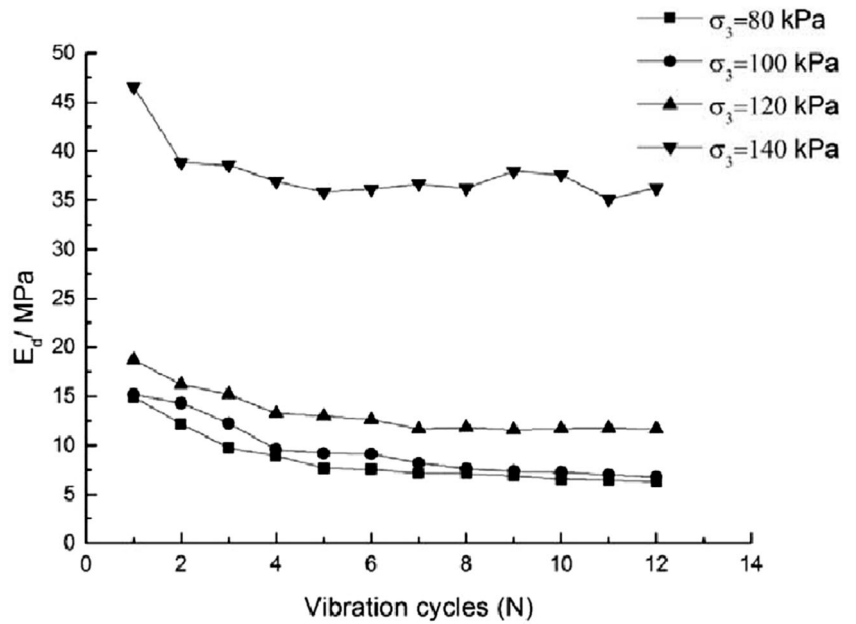


Table 7: the directional probability entropy of undisturbed loess structural units is small, so their directionality is better. After dynamic loading, the directional probability entropy of the structural units has an increasing tendency (on the whole); however the change is not obvious, which indicates that the dynamic load has little effect on the directionality of the structural units.

Average shape factor

According to Eq. (3), the average shape factor (F) of structural units in each sample can be calculated (Table 8): analysis

shows that, compared with undisturbed soil samples, the average shape factor changes little after the action of dynamic load, and has an increasing tendency on the whole. This shows that the shape of the structural units tended to be oblate with increasing confining pressure. Combined with the directionality analysis of the structural units, although the directional probability entropy had an increasing tendency after the action of dynamic load, the structural unit directionality of each specimen was improved, and thus the oblate shape of the units was more conducive to the formation of a stable structure, therefore improving the dynamic elastic modulus.

Fig. 7 $E_{dmax} - \sigma_3$ curve

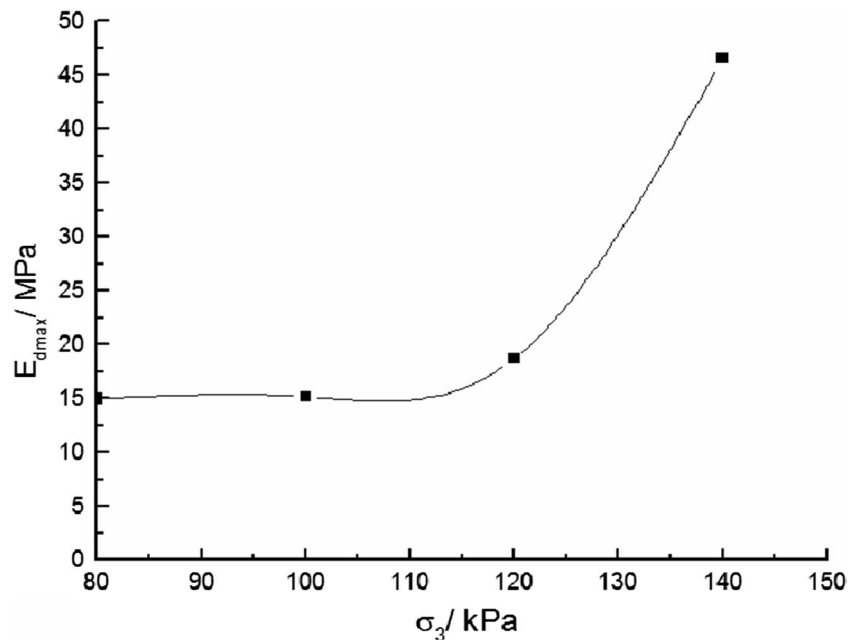
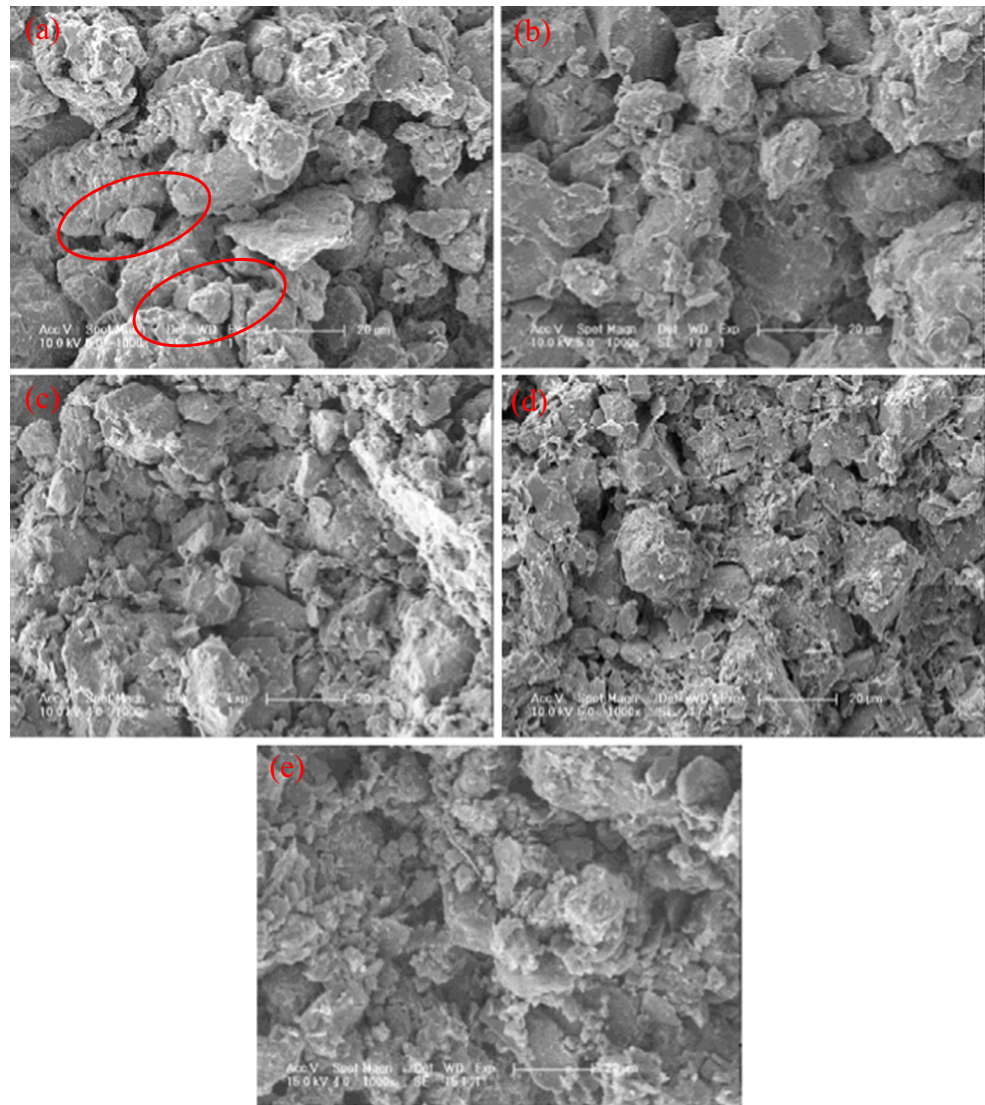


Fig. 8 Microstructure photographs of soil specimens under different confining pressures (a) Undisturbed loess (b) Specimen 1 (c) Specimen 2 (d) Specimen 3 (e) Specimen 4



Fractal dimension of the morphology

Based on Eq. (4), the fractal dimension of morphology (B) of the structural units can be obtained (Fig. 9). The results show that, with increasing confining pressure, B continually increased, and when the confining pressure was low, the change was small, but was bigger when the confining pressure was high. The increase

in B indicated that, with the increase in confining pressure, the surface undulation of units became larger and the surface was rougher. This arose because, under the action of external load, small particles were attached to the surfaces of the larger ones, which made the larger particles rougher, and it also increased the friction between units, which was consistent with the measured change in macroscopic strength.

Table 6 The distribution of equivalent diameter (%) and average diameter (μm) of units

Specimen number	Equivalent diameter of structural units/ μm				Average diameter/ μm
	≥ 10	10 to 5	5 to 2	≤ 2	
Undisturbed specimens	23.28	46.13	12.36	18.23	11.056
1	21.91	46.05	12.98	19.06	10.782
2	21.17	45.79	12.70	20.34	8.576
3	20.86	44.91	13.17	21.06	7.245
4	19.51	43.96	12.51	24.02	6.913

Table 7 Directional probability entropy of structural units

Specimen number	Undisturbed specimens	1	2	3	4
H _m	0.559	0.576	0.523	0.556	0.585

Rate of internal pore

According to Eq. (5), *R* can be calculated for each sample (Table 9). The results show that, compared with the undisturbed sample, *R* changes little after dynamic loading, and at low confining pressures *R* remains almost unchanged, but decreases slightly at high confining pressures. This is consistent with the destruction of the larger structural units under high confining pressure and arose because, when the confining pressure was high, some of the grain aggregates were compressed or destroyed, but due to the internal pores being small, and fewer in number, *R* changed little.

Quantitative analysis of pores

Equivalent diameter

Lei (1987) measured the pores in loess through mercury intrusion porosimetry (MIP), combined with the grain component characteristics of loess, pores in loess were divided into four types according to their equivalent diameter: macropores ($d > 16 \mu m$), mesopores ($4 \mu m < d \leq 16 \mu m$), fine pores ($1 \mu m < d \leq 4 \mu m$) and micropores ($d \leq 1 \mu m$). Accordingly, the pores in each sample were classified and their amount calculated.

The equivalent diameter distribution and average diameter of pores are shown in Table 10: the average pore diameter constantly decreases with increasing confining pressure, and the pores tend to become smaller on the whole. At $\sigma_3 = 80$ kPa, the pore composition is almost unchanged. At low confining pressures, more mesopores are damaged, but macropores remain essentially intact; however at high confining pressures, the macropores content decreased obviously.

In the testing process, there are three cases of macropore development in samples: a reduction in pore size caused by compression, leading to a decrease in the macropore

content; further expansion of pore size owing to the destruction of the structure produced by the applied dynamic load, which increases the macropore content; the filling of macropores owing to the generation of small particles, causing a reduction in the macropore content. As shown in Table 10: compared with the undisturbed sample, when the confining pressure was 80 kPa, the macropore content decreased slightly, and it remained relatively unchanged when the confining pressures were 100 and 120 kPa. When the confining pressure was 140 kPa, the macropore content decreased because the development pattern of pores in samples changed with testing conditions. On the one hand, under the effect of the confining pressure, the macropore content will decrease with increasing pressure. On the other hand, the higher the confining pressure, the denser the consolidated sample tends to be, so the greater damage generated in the structure under dynamic load at failure. The damage to the structure causes an increase in the macropore content, meanwhile, it results in the destruction of the original connection between particles, leading to the generation of fine particles which may fill up the macropores, thus decreasing the macropore content. When the confining pressure was 80 kPa, the macropore content was principally controlled by the consolidation process because of the low confining pressure, and it presented a reducing trend thereafter. With increasing confining pressure, the damage to the structure under dynamic load was exacerbated, causing an increase in the macropore content when the fine particles were generated; however, when the confining pressure was 140 kPa, the sample contained the highest content of newly-generated small particles (equivalent diameter $\leq 2 \mu m$) as shown in Table 6, so the macropores were well-filled by these particles, and thus the macropore content decreased.

As mentioned above, at a confining pressure of 140 kPa, the dynamic elastic modulus of the specimens is greatly improved, but when the confining pressures are 80 kPa, 100 kPa or 120 kPa, the dynamic elastic modulus changed little, so damage to macropores improved the dynamic strength of this soil.

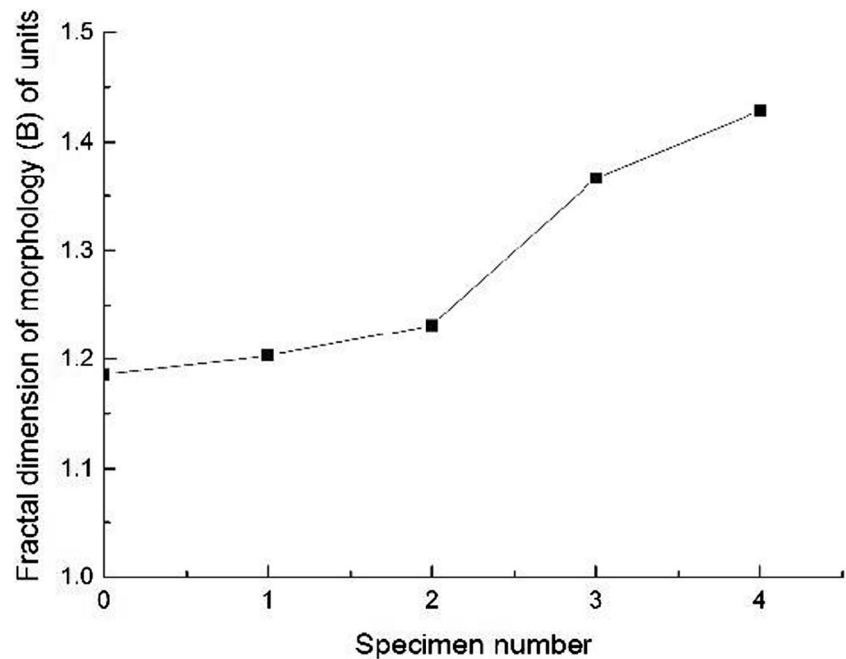
Directional probability entropy

According to Eq. (2), the directional probability entropy of pores can be obtained (Fig. 10): compared with the

Table 8 Average shape factor of the structural units

Specimen number	Undisturbed specimens	1	2	3	4
F	0.593	0.573	0.608	0.597	0.629

Fig. 9 Relationship between the fractal dimension of the morphology of the structural units and specimen number (specimen 0 is the undisturbed loess)



undisturbed sample, the directional probability entropy of the pores decreases after dynamic loading. With increasing confining pressure, the directional probability entropy decreases constantly, but the decrement is small. The results show that the greater the confining pressure, the better the directionality of the pores.

Average shape factor

According to Eq. (3), the average shape factor of pores can be obtained (Table 11): the average shape factor of the pores has a decreasing trend after dynamic loading, but there is no

Table 9 Rate of internal pore for structural units

Specimen number	Undisturbed specimens	1	2	3	4
R	4.46	4.63	4.20	4.12	3.53

obvious regularity thereto. This shows that the shape of the pores had become long and narrow after dynamic loading, but that was not related to the change in confining pressure. This may be influenced by the shape of the structural units: after they became oblate, the pores became longer and narrower.

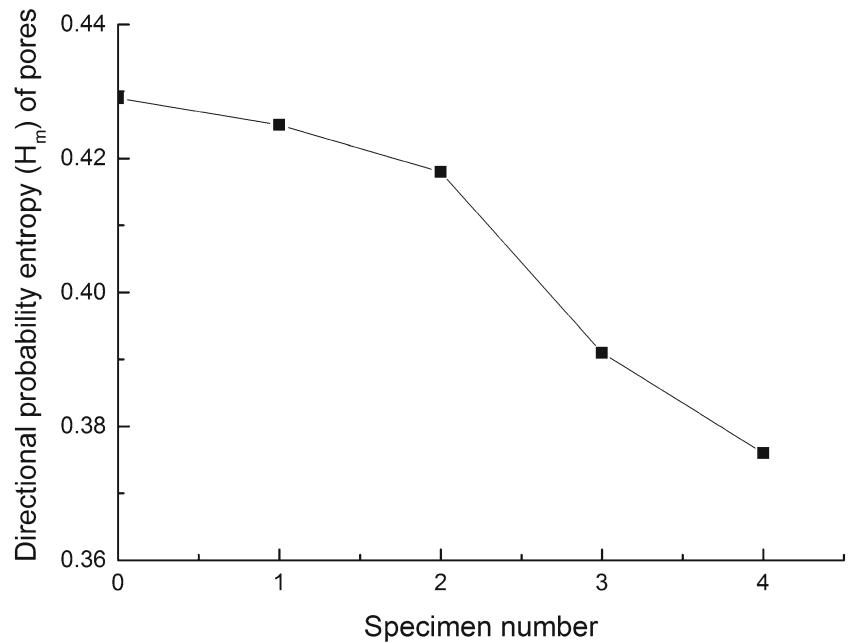
Fractal dimension of the morphology

According to Eq. (4), the equivalent perimeter and equivalent area of the pores are fitted, and the fractal dimension of their morphology can be obtained (Fig. 11): the fractal dimension of the morphology increases after vibration, and has a positive correlation with confining pressure. The results indicate that the fluctuation of the microcosmic surfaces of the pores increases, and the structure becomes more complicated. The morphological characteristics of the pores are principally dependent on the morphology of the structural units, and the surface fluctuation of the structural units increases with increasing confining pressure, so the structure of the pores becomes complicated.

Table 10 Distribution of equivalent diameter (%) and average diameter (μm) of pores

Specimen number	Equivalent diameter of pores/ μm				Average diameter/ μm
	≥ 16	6 to 4	4 to 1	≤ 1	
Undisturbed specimens	1.97	16.07	79.02	2.95	3.153
1	1.64	16.78	79.61	1.97	3.076
2	1.98	11.64	83.79	2.59	2.956
3	2.00	11.25	84.50	2.25	2.901
4	0.64	10.41	86.26	2.69	2.805

Fig. 10 Relationship between the directional probability entropy of pores and specimen number (specimen 0 is the undisturbed loess)



Analysis of the relationship between microstructural parameters and dynamic elastic modulus

To explore the relationship between the dynamic characteristics and microstructure of saturated loess under different confining pressures, the dynamic elastic modulus was chosen as a representative parameter of macroscopic strength. Grey correlation theory is used to evaluate the correlation between the microstructural parameters and dynamic elastic modulus, to reveal those microstructural parameters affecting the dynamic elastic modulus of this saturated loess, so the relationship between them can be fitted.

Correlation analysis based on grey relational theory

Grey relational analysis is used to serialise the grey relationship where the physical model and operating mechanism are unclear; it can be determined whether the two are relevant, and if they are relevant, the correlation between them can be evaluated. Here, the distribution of microstructural parameters was irregular, the relationship between the microstructural parameters and dynamic elastic modulus remained unclear; because there are many microstructural parameters that have to be evaluated, if the method used to fit the empirical formula is used to evaluate the correlation between the microstructural parameters and the dynamic elastic modulus, the first step is to fit the empirical formula, and then inspect the confidence level of the formula through various methods. Compared with grey relation theory, it suffers disadvantages in that the processing result is inaccurate and computationally expensive; so it was more appropriate to analyse it through grey relational theory. The basic principle of the theory aims to compare the

similarity of geometries between reference sequences and comparative sequences: the closer the geometry of the sequence plot and the change therein, the greater the degree of correlation, and vice versa. The definition of the degree of correlation follows (Lin 2007).

Assume that there are *n* sub factors *X_i*, which are related to the generating factors *X₀*, and they all have at least *N* values from dynamic observations in the same period, and they are, respectively, the comparative sequence and the reference sequence.

$$\text{Reference sequence : } X_0 = \{X_0(k), k = 1, 2, \dots, m\}$$

$$\text{Comparative sequence : } X_i$$

$$= \{X_i(k), k = 1, 2, \dots, m; i = 1, 2, \dots, n\}$$

$\xi_i(k)$ is the correlation coefficient between *X₀* and *X_k* at the *Kth* point, and it can be calculated by using Eq. (6):

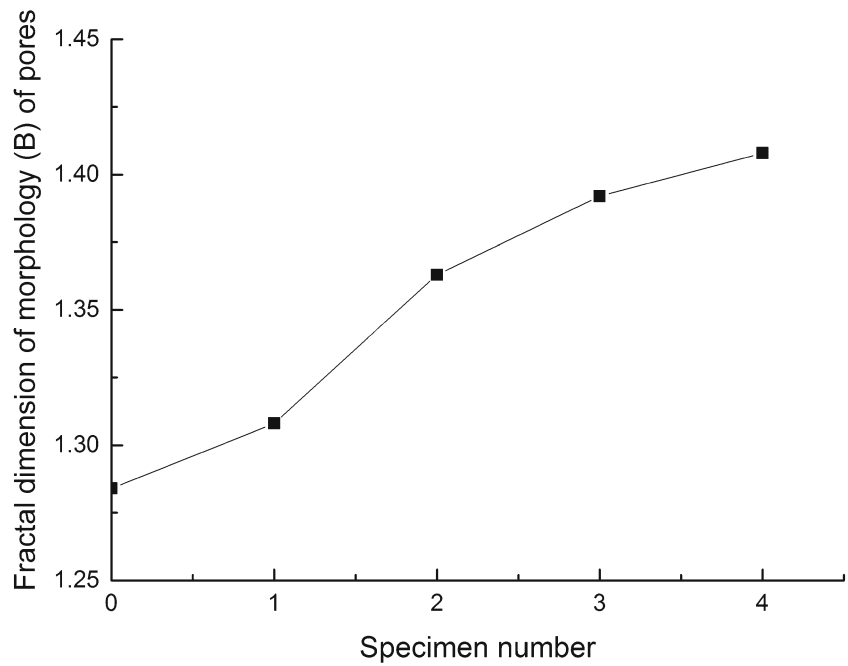
$$\xi_i(k) = [min_k |X_i(k) - X_0(k)| + \rho max_k |X_i(k) - X_0(k)|] / [min_k |X_i(k) - X_0(k)| + \rho max_k |X_i(k) - X_0(k)|] \tag{6}$$

Where ρ is an identification coefficient in the range (0,+∞). The smaller the value of ρ , the greater the resolution ratio, in general $\rho = 0.5$. The degree of correlation (γ_i) can be calculated by using Eq. (7):

Table 11 Average shape factor of pores

Specimen number	Undisturbed specimen	1	2	3	4
F	0.510	0.459	0.460	0.483	0.472

Fig. 11 Relationship between the fractal dimension of the morphology of the pores and specimen number (specimen 0 is the undisturbed loess)



$$\gamma_i = \frac{1}{n} \sum_{k=1}^n \xi_i''(k) \tag{7}$$

Here, $\rho = 0.5$, at this time it is generally believed that the two factors are correlated when $\gamma_i \geq 0.6$, and the greater γ_i , the stronger the correlation. When $\gamma_i < 0.6$, the correlation is poor (Lin 2007).

The degree of correlation between the microstructural parameters and the dynamic elastic modulus is calculated using MATLAB™. The original data for structural units, pores, and

the dynamic elastic modulus of specimens are shown in Table 12.

The degree of correlation is shown in Table 13; in addition to the average shape factor of the pores, the approximate microstructural parameters were all correlated to the dynamic elastic modulus, and the correlation between the directional probability entropy and dynamic elastic modulus was much lower. The fractal dimension of their morphology and the average shape factor of the structural units and the average diameter of pores are highly correlated to the dynamic elastic modulus (with degrees of correlation exceeding 0.8) (Zhao 2008).

Table 12 Original data: microstructural parameters and dynamic elastic modulus

Specimen number	Structural units					Pores				
	$\bar{D} / \mu\text{m}$	F	H_m	B	R	$\bar{D} / \mu\text{m}$	F	H_m	B	E_d / MPa
1	10.782	0.573	0.576	1.203	4.630	3.076	0.495	0.425	1.308	6.750
2	8.576	0.608	0.523	1.232	4.200	2.956	0.460	0.418	1.363	7.390
3	7.245	0.597	0.556	1.367	4.120	2.901	0.483	0.391	1.392	11.720
4	6.913	0.629	0.585	1.429	3.530	2.805	0.472	0.376	1.408	36.630

Table 13 Degree of correlation between microstructural parameters and dynamic elastic modulus

Study object	$\bar{D} / \mu\text{m}$	F	H_m	B	R
Structural units	0.724	0.832	0.662	0.856	0.755
Pores	0.875	0.594	0.656	0.773	/

Table 14 Parameter value and fitted value

E_d /MPa	\bar{D} / μm	F	B	Fitted value/MPa
6.75	3.076	0.573	1.203	6.758
7.39	2.956	0.608	1.232	7.396
11.72	2.901	0.597	1.367	11.678
36.63	2.805	0.619	1.429	36.570

Fitting of the relationship

The correlation analysis shows that the average diameter (\bar{D}) of the pores, the average shape factor (F) and the fractal dimension of their morphology (B) of the structural units are most significantly correlated to the dynamic elastic modulus among all the microstructural parameters. SPSS software was used to fit on the basis of Eq. (8), and the multiple linear regression method was chosen for subsequent analysis. Assuming that the dynamic elastic modulus was the dependent variable and \bar{D} , F , and B were independent variables:

$$E_d = b_0 + b_1\bar{D} + b_2F + b_3B \quad (8)$$

Multiple linear regression is a regression between one dependent variable and two or more than two independent variables. The multiple linear regression model used in this paper is as follows:

$$y_i = b_0 + b_1x_{1i} + b_2x_{2i} + \dots + b_mx_{mi} + \varepsilon_i \quad (9)$$

Where b_0, b_1, \dots, b_m are undetermined estimators, ε_i is the mutual independence and weight-equivalent random error component, which has n values.

The fitting result gave:

$$E_d = 3048\bar{D} + 8818F + 1992B - 16817.98 \quad (10)$$

The parameter values for fitting, and the fitted values, are shown in Table 14. The maximum error between the actual values and fitted values was 0.35%, which indicated that Eq. (9) offered a good, high-precision, prediction. It can be considered that the average shape factor (F) makes the greatest contribution on the dynamic strength, and the fractal dimension of the morphology (B) the smallest.

Conclusion

Through the above analysis and research, the following conclusions can be drawn:

- (1) The dynamic elastic modulus of a saturated loess in Xianyang decreases gradually with increasing vibration cycle and tends to be stable, the stable value changes little when the confining pressure is low, but increases greatly at high confining pressures. The maximum dynamic elastic modulus increases with increasing confining pressure, and the increment is small under low confining pressures, but greater at higher confining pressures.
- (2) The undisturbed loess has a skeletal structure which remains unchanged when the confining pressure increases. The contact between particles gradually transforms from a point contact to a surface contact.
- (3) The equivalent diameter of the structural units is concentrated within the range 5 to 10 μm , their number decreases with increasing confining pressure, also the number of units exceeding 10 μm greatly decreases, but the number less than 2 μm increases. The soil is denser at high confining pressures. The average shape factor and the directional probability entropy of structural units are all slightly increased, and the fractal dimension of their morphology increased, but the rate of internal pore decreases slightly at high confining pressures.
- (4) With increasing confining pressure, the main change in the pores saw an increase in the number of fine pores, a decrease in the number of mesopores, and a greater decrease of macropore numbers under higher confining pressures. The average shape factor and directional probability entropy of pores decrease with increasing confining pressure, but the fractal dimension of their morphology increases.
- (5) In addition to the average shape factor of pores, the approximate microstructural parameters were all correlated to the dynamic elastic modulus. The average diameter of pores, the fractal dimension of the morphology and the average shape factor of the structural units were significantly correlated to the dynamic elastic modulus, and the dynamic elastic modulus values were fitted with the three aforementioned parameters.

Acknowledgements This work was supported by the National Natural Science Foundation of China (Nos. 41472242 and 41402243).

References

- ASTM D2487-11 (2011) Standard Practice for Classification of Soils for Engineering Purposes (Unified Soil Classification System). US-ASTM
- Giménez RG (2012) Characterization of loess in central Spain: a microstructural study. *Environmental Earth Sciences* 65(7):2125–2137. doi:10.1007/s12665-011-1193-7

- Hu RL, Yeung MR, Lee CF, Wang SJ (2001) Mechanical behavior and microstructural variation of loess under dynamic compaction. *Eng Geol* 59(3–4):203–217. doi:[10.1016/S0013-7952\(00\)00074-0](https://doi.org/10.1016/S0013-7952(00)00074-0)
- Jiang MJ, Zhang FG, Hu HJ et al (2014) Structural characterization of natural loess and remolded loess under triaxial tests. *Eng Geol* 181: 249–260. doi:[10.1016/j.enggeo.2014.07.021](https://doi.org/10.1016/j.enggeo.2014.07.021)
- Lei XY (1987) Pore types and collapsibility of loess in China. *Chinese Science* 17(12):1309–1318
- Li SL (1990) Principles and methods of dynamic triaxial tests. Geological Press, Beijing
- Li RD (2004) The study of dynamic characteristics of loess in Dongshan Taiyuan. MSC Dissertation, Taiyuan University of Technology (in Chinese)
- Lin WY (2007) Correlation analysis of physical and mechanical properties of rock and soil. *China Rural Water Conservancy and Hydropower* 2:27–32
- Liu DS (1965) Loess accumulation in China. Science Press, Beijing
- Luo YS et al (2004) GB 50025–2004. Standards for construction in collapsible loess area. China Architecture & Building Press, Beijing
- Moore CA, Donaldson CF (1995) Quantifying soil microstructure using fractals. *Géotechnique* 45(1):105–116
- Mosallamy ME, Fattah TTAE, Khoully ME (2015) Experimental study on the determination of small strain-shear modulus of loess soil. *HBRC J* 35(2):181–190. doi:[10.1016/j.hbrcj.2014.11.010](https://doi.org/10.1016/j.hbrcj.2014.11.010)
- Osipov B (1985) The nature of strength and deformation properties of clay soil and rocks. Geological Press, Beijing
- Shi B (1997) Quantitative study on microstructure directionality of cohesive soil. *Acta Geol Sin* 71(1):36–44
- Shi YC (2003) Study on characteristics of earthquake parameters and its application in loess area. Ph.D Dissertation, Lanzhou University (in Chinese)
- Terzaghi K, Peck RB (1948) Soil mechanics in engineering practice. Wiley, New York
- Wang Q, Wang JP (2000) Study on fractal geometry of soil pores. *Chinese J Geotech Eng* 22(4):496–498
- Wang NQ, Liu XL, Luo DH et al (2012a) Study on dynamic strength characteristics of Malan loess. *Appl Mech Mater* 170-173:964–968. doi:[10.4028/www.scientific.net/AMM.170-173.964](https://doi.org/10.4028/www.scientific.net/AMM.170-173.964)
- Wang Q, Wang LM, Wang J et al (2012b) Laboratory study on the liquefaction properties of the saturation structural loess. *Appl Mech Mater* 170-173:1339–1343. doi:[10.4028/www.scientific.net/AMM.170-173.1339](https://doi.org/10.4028/www.scientific.net/AMM.170-173.1339)
- Wang NQ, Liu XL, Han B et al (2013) Test of dynamic strength characteristics of Lishi loess. *Appl Mech Mater* 303:2902–2907. doi:[10.4028/www.scientific.net/AMM.303-306.2902](https://doi.org/10.4028/www.scientific.net/AMM.303-306.2902)
- Wang JD, Ren Q, Gu TF, Xu YJ (2014) The text analysis on the relationship between slide-zone loess porosity microstructure and dynamic parameters. *Appl Mech Mater* 638-640:633–638. doi:[10.4028/www.scientific.net/AMM.638-640.633](https://doi.org/10.4028/www.scientific.net/AMM.638-640.633)
- Xiao ZH, Han B, Liao HJ et al (2009) Experiment study on dynamic strength of loess under repeated load. *Int J Mod Phys B* 22(31n32):453–458. doi:[10.1142/S0217979208051236](https://doi.org/10.1142/S0217979208051236)
- Yan FX, Huang XZ (2014) Dynamic and static mechanical properties of loess subgrade in Shanxi. *Geo-Shanghai*:39–44
- Yuan ZH (2015) Study on the strength and the microstructure change of loess under dry-wet cycle. Ph.D Dissertation, Chang'an University (in Chinese)
- Zhang KX, Xie JW (1989) Soil dynamics. Seismic Press, Beijing
- Zhao AP (2008) Study on microcosmic mechanism of frost heave of subgrade soil in seasonal frozen region. Ph.D Dissertation, Jilin University (in Chinese)